

Supplemental Material - Resolving Vibrational from Electronic Coherences in Two-Dimensional Electronic Spectroscopy: The Role of the Laser Spectrum

Franco V. de A. Camargo,^{1,2} Lena Grimmelsmann,^{1,3} Harry L. Anderson,⁴ Stephen R. Meech,¹ and Ismael A. Heisler¹

¹*School of Chemistry, Norwich Research Park,
University of East Anglia, Norwich NR4 7TJ, United Kingdom*

²*CAPES Foundation, Ministry of Education of Brazil, Brasilia DF 70040-202, Brazil*

³*Fakultät für Chemie und Biochemie, Ruhr-Universität Bochum,
Universitätsstrasse 150, 44801, Bochum, Germany*

⁴*Department of Chemistry, Chemistry Research Laboratory,
University of Oxford, Oxford OX1 3TA, United Kingdom*

(Dated: December 13, 2016)

SAMPLE DETAILS

The 5,15-bisalkynyl zinc porphyrin monomer studied in this work was synthesised as in reference [1]. For the experiments reported here it was dissolved in *n*-pentane with 1% by volume of pyridine to suppress aggregation. The concentration was $\sim 330 \mu\text{M}$ in a $200 \mu\text{m}$ static pathlength cell, corresponding to a maximum optical density in the *Q* band of 0.25. In order to be sure there was no aggregation we compared the linear absorption spectra between the samples and solutions at lower concentrations. We also found that adding more pyridine had no effect. Control measurements flowing the sample were performed and yielded identical results. Figure S1 shows the full wavelength scale linear absorption spectrum with the *Q* band assignments from reference [2]. The molecular structure and the transition dipole moment orientation are shown on the inset of Figure S1.

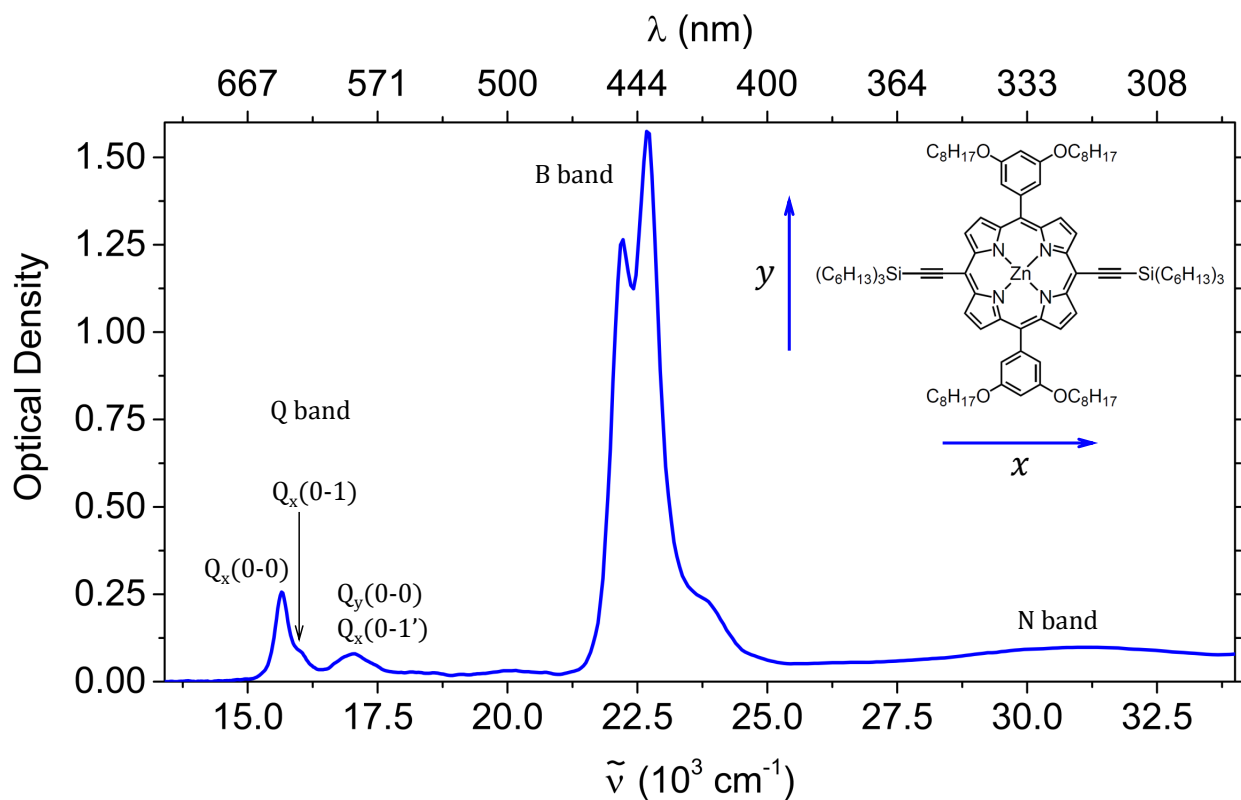


Figure S1. Linear absorption of the porphyrin monomer in the visible and near UV. Inset: structure of the porphyrin monomer and transition dipole moment orientation in the molecular frame.

2D-ES EXPERIMENTAL SETUP

The 2D-ES spectrometer used in this study has been described in detail in reference [3]. 2D-ES, like one dimensional transient absorption techniques, detects four-wave mixing signals (that is, there are three interactions between the excitation lasers and the sample, followed by a signal emission). The essential feature of 2D-ES is to use three ultrashort excitation pulses and detect only pathways for which each field-matter interaction takes place with a different pulse within the limits of pulse duration – below 15 fs in our case. Then the time delay between the first and second interactions can be experimentally controlled and the signal can be acquired as a function of this delay, during which the system’s density matrix is in a coherence between the ground and an electronic excited state. For this reason this time period is called the coherence time (τ) and if a Fourier transform is applied on this variable, the corresponding frequency is the excitation frequency (ν_1), which we report in wavenumber ($\tilde{\nu}_1$). The signal is heterodyne-detected spectrally dispersed, so we recover the emission frequency, which we also report in wavenumber ($\tilde{\nu}_3$). Therefore, for any chosen value of the population time delay T (which is the delay between the second and third pulses), a correlation map between ($\tilde{\nu}_1, \tilde{\nu}_3$) can be recovered.

The main challenge in experimentally performing 2D-ES measurements is to keep phase stability, which is a very stringent requirement because during the coherence time the sample is in a coherent superposition between the ground and an electronic excited state, so phase stability within the optical cycle is in principle required. Many different experimental approaches have been demonstrated which satisfy the requirements [4], and ours is an extension of a development by the Brixner group which employs only conventional optics [5]. The optical design responsible for the phase-locking, originally demonstrated by the Miller group [6], has different pairs of beams hitting the same optics in such a way that their phase fluctuations become anti-correlated, leading to an overall cancellation.

Briefly, the light source consists of a commercial noncollinear parametric amplifier (NOPA) pumped by an amplified laser system at 10 kHz. The pulses are recompressed close to the Fourier transform limit by prism compressors, and characterized at the sample position by transient grating frequency resolved optical gating (TG-FROG) using a fused silica window. A sketch of the experimental apparatus is shown in Figure S2. The four beams (three pump beams plus an attenuated local oscillator) are generated by beamsplitters and

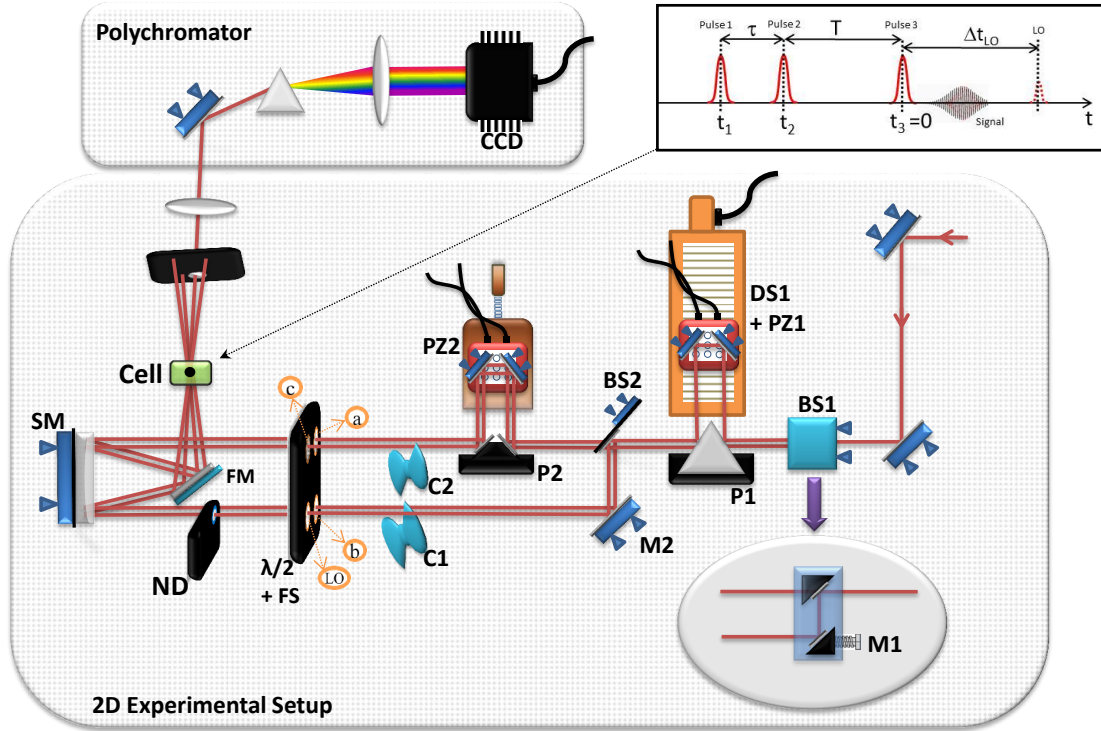


Figure S2. Sketch of the 2D-ES spectrometer. BS1,2 beamsplitters; P1,2 aluminium coated knife-edge right angle prisms; DS1 and PZ1,2 mechanical delay stages; C1,2 optical choppers; $\lambda/2 + \text{FS}$ half wave plates plus fused silica windows; ND neutral density filter; SM spherical mirror; FM folding mirror. The upper right corner illustrates the pulse arrival sequence on the sample as well as the signal emission and LO position in time relative to pulse c. In the upper left the homemade polychromator is shown, composed of a mirror, a highly dispersive prism, a lens and the CCD camera.

propagate on the corners of a 2.5 cm square before being focused on the sample. The order of arrival of the first two pulses determines whether the rephasing or non-rephasing signal is emitted at the direction of the detector. The movement of the delay stages for this design is in the full rotating wave frame. This means that a phase is introduced on the beams which compensates the oscillation at the optical cycle, meaning that a large reduction in the number of τ scanning points is achieved [7]. In our case, τ was scanned from -150 to 150 fs in steps of 5 fs.

The main difference between this setup and the original is that we introduced two chop-

pers and a single-line CCD camera for detection. This enables us to better remove scattering, detect in an almost shot-to-shot regime (we use bundles of 5 shots), and also acquire the broadband transient absorption spectrum quasi-simultaneously with the 2D [3]. As a result we recover one 2D-ES spectrum per minute, including the local oscillator and transient absorption spectra. The signal is heterodyne detected, and through the use of a phasing routine based on the projection-slice theorem, the complex-valued 2D-ES spectra can be recovered. The main advantage of this setup is the fast data acquisition with very good signal over noise.

LIOUVILLE-SPACE PATHWAYS

Displaced Harmonic Oscillator

Here we show all the Liouville-space pathways diagrams which are expected to give the largest signal contributions for a displaced harmonic oscillator energy level structure. We make the assumption that all pathways start from a density matrix $|g_0\rangle\langle g_0|$ and only and only the two lowest levels in the vibrational ladder are involved. In the diagrammatic representation of the Liouville-space pathways the vertical axis represents time, and each field-matter interaction is associated with an arrow connecting to the density matrix. If the arrow points towards the density matrix it represents an excitation, and if it points away from the density matrix, it represents a de-excitation. Arrows pointing to the left (right) carry negative (positive) phase and wave vector. If the first, second and third field matter interactions take place with pulses labelled 1, 2 and 3 respectively, then rephasing signals have phase-matching $-\mathbf{k}_1 + \mathbf{k}_2 + \mathbf{k}_3$, while non-rephasing diagrams have phase-matching $\mathbf{k}_1 - \mathbf{k}_2 + \mathbf{k}_3$, where \mathbf{k}_j , with $j \in \{1, 2, 3\}$, represents the wave vector of each field. Signal emission is drawn with a dashed arrow and the density matrix at each experimental time interval is explicitly included, with the leftmost diagrams in each Figure including labels marking the beginning of each time interval.

As discussed in the main text, only pathways for which all field-matter interactions and signal emission lie within the laser spectrum will be observed. Therefore, we explicitly write the wavenumber of each interaction in the right hand side of each diagram, and when it takes place at a frequency red-shifted from the main absorption (that is, outside the spectrum of experiment 2 in the main text) it is placed inside a red box, with the corresponding arrow drawn in red, to emphasize this transition may not be covered by the laser spectrum. When a coherence during T is present, it will modulate the 2D-ES signal with a frequency that can be either positive or negative, and in our case $|g_n\rangle\langle g_{n+1}|$ coherences have positive sign, while $|g_{n+1}\rangle\langle g_n|$ have negative sign, which are marked with green and red $\tilde{\nu}_0$ symbols respectively (Figures S5, S6, S10 and S11).

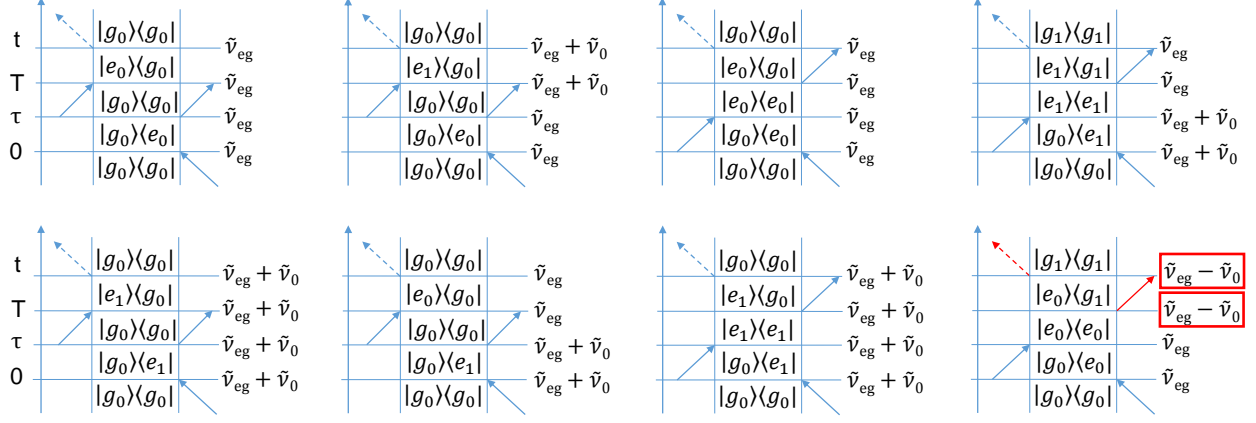


Figure S3. Rephasing population Liouville-space pathways for the displaced harmonic oscillator model. On the right hand side of each diagram the wavenumber of each interaction is explicitly shown and a red box encloses it in case it lies outside the spectral coverage of experiment 2 from the main text. In this case, the arrow corresponding to that interaction is also displayed in red.

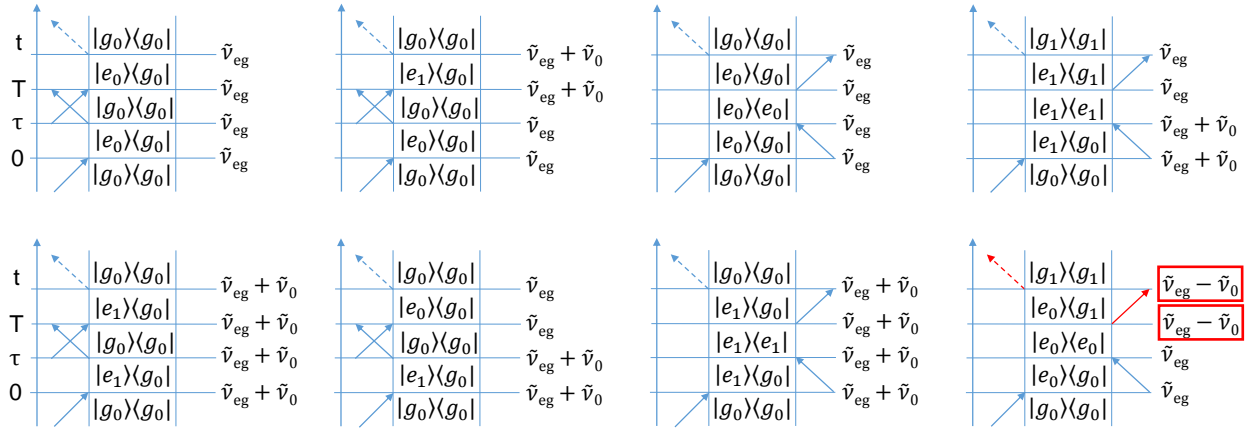


Figure S4. Non-rephasing population Liouville-space pathways for the displaced harmonic oscillator model. See caption of Figure S3 for details.

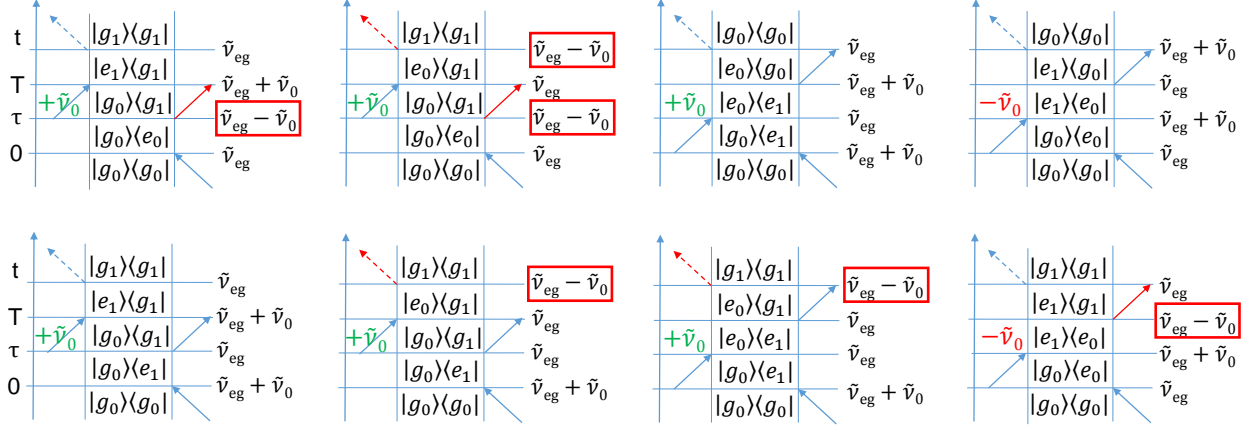


Figure S5. Rephasing oscillatory Liouville-space pathways for the displaced harmonic oscillator model. See caption of Figure S3 for details.

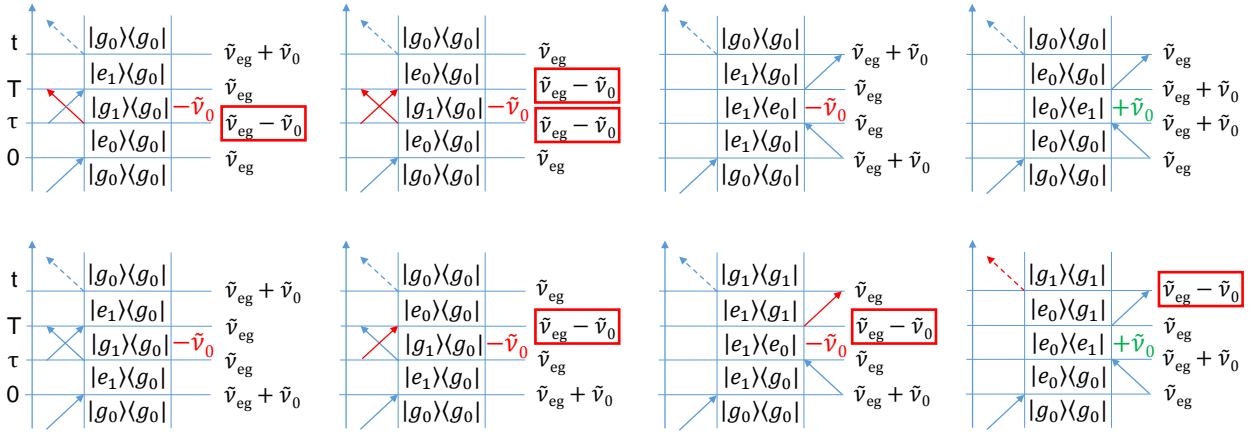


Figure S6. Non-rephasing oscillatory Liouville-space pathways for the displaced harmonic oscillator model. See caption of Figure S3 for details.

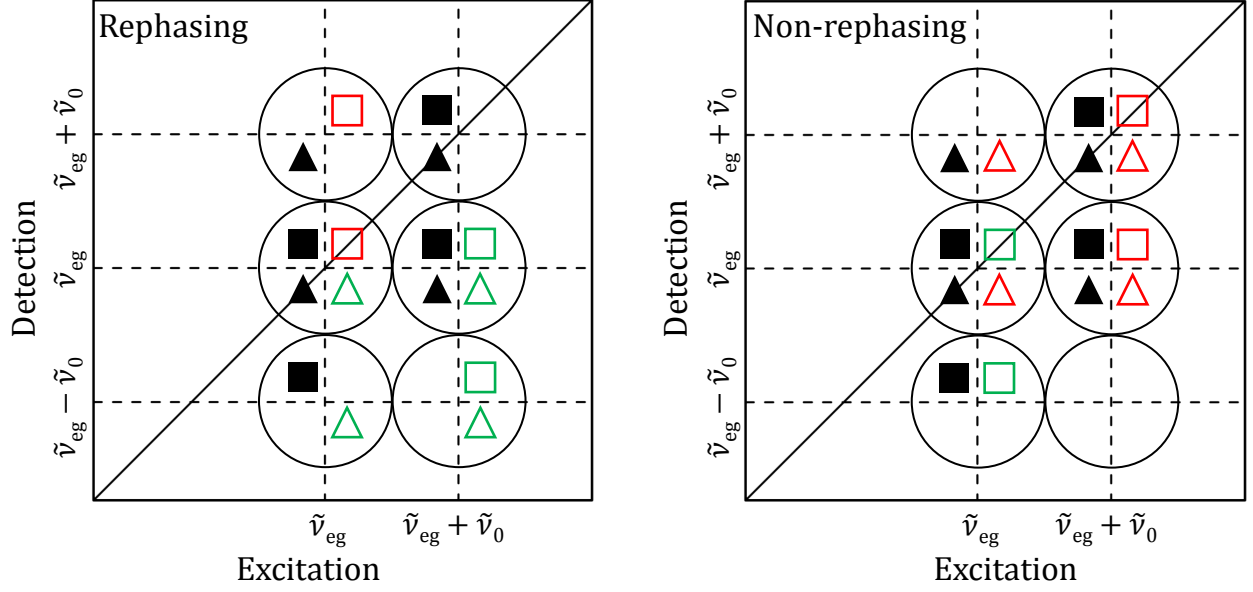


Figure S7. Scheme of Liouville-space pathways (extending Figures 3a,b from the main text to include population pathways) in rephasing (left) and non-rephasing (right) 2D maps for experiment 1. Each geometric figure marks a pathway, with squares representing an excited state and triangles representing a ground state population during T . Black geometric figures correspond to non-oscillatory pathways, whereas oscillatory ones are marked with open diagrams, which are red if the corresponding frequency is negative and green if it is positive. The signal corresponding to each geometric figure is centred in the black circle within which the figure is contained.

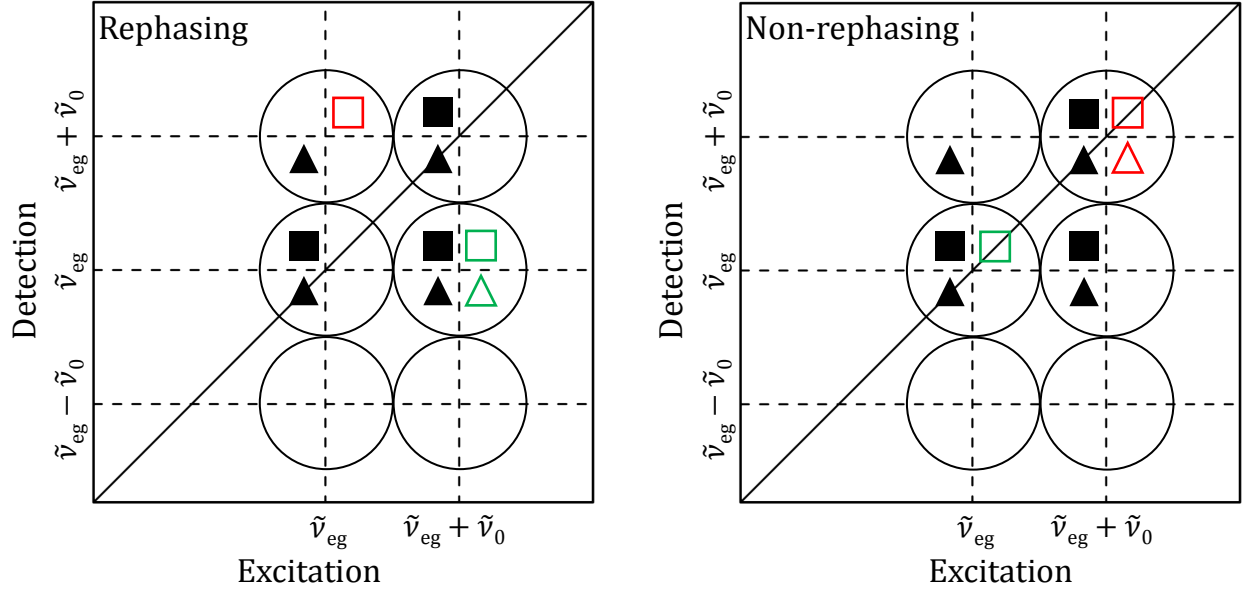


Figure S8. Scheme of Liouville-space pathways (extending Figures 4a,b from the main text to include population pathways) in rephasing (left) and non-rephasing (right) 2D maps if the frequency $\tilde{\nu}_{eg} - \tilde{\nu}_0$ is not present in the laser spectrum, corresponding to experiment 2. See caption of Figure S7 for details.

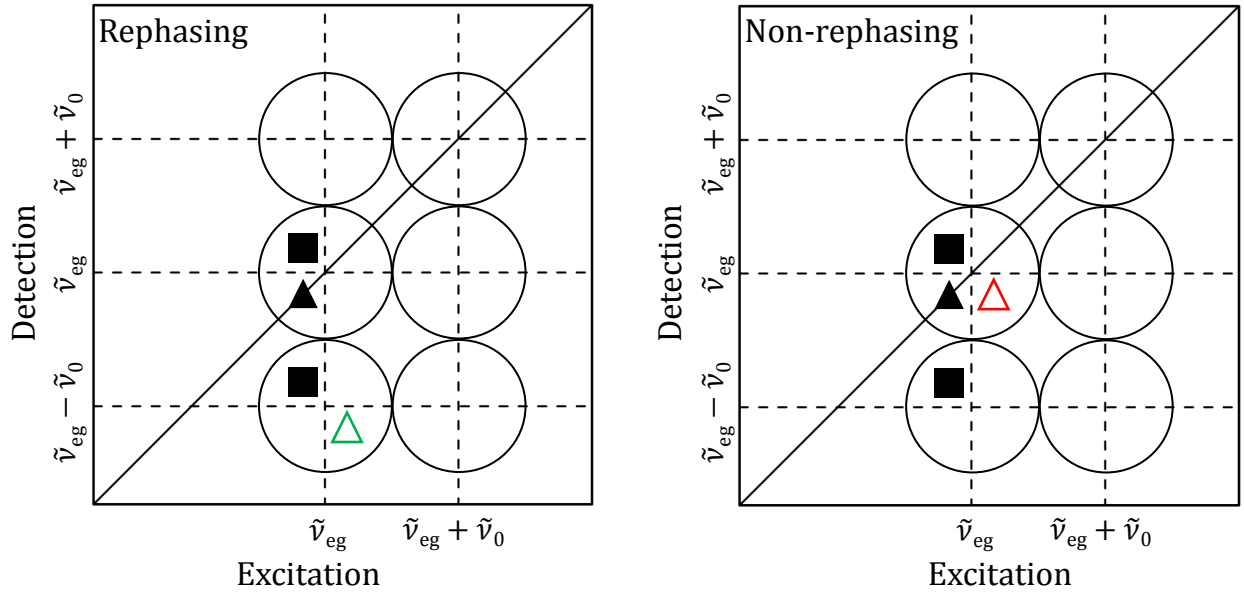


Figure S9. Scheme of Liouville-space pathways in rephasing (left) and non-rephasing (right) 2D maps (see caption of Figure S7 for details) if the laser spectrum has amplitude at $\tilde{\nu}_{eg} - \tilde{\nu}_0$, but not at $\tilde{\nu}_{eg} + \tilde{\nu}_0$ (vibronic peak in the linear absorption). The Q_x band of the porphyrin monomer is coupled to a vibrational mode at 1340 cm^{-1} , for which experiment 1 falls in this regime.

Purely Electronic Coherences

In this section we show all Liouville-space pathways for the energy level scheme displayed in Figure 2b from the main text, where electronic coherences between $|e'\rangle$ and $|e''\rangle$ can be prepared. We note that usually the comparison between the displaced harmonic oscillator model and an excitonic dimer is made. For an excitonic dimer, the two energetically close excited states arise from dipole-dipole coupling between two chromophores, which also results in the appearance of a doubly excited state at twice the energy. The presence of another sharply defined transition from $|e'\rangle$ or $|e''\rangle$ to a higher excited state in resonance with the laser gives rise to excited state absorption (ESA) pathways. In our specific case of the porphyrin monomer this picture does not apply, but nonetheless there are two independent excited states close in energy, namely the Q_x and the Q_y bands, and because both appear in the linear absorption a coherent superposition of both can in principle be prepared by broadband laser excitation. Therefore we do not consider higher excited states here. We do point however that the pathways which arise through the presence of a double exciton level overlap with the others, resulting in no new peak positions in 2D maps [8]. Comparison between Figures S8 and S12 shows how similar the signatures of electronic and vibrational coherences are.

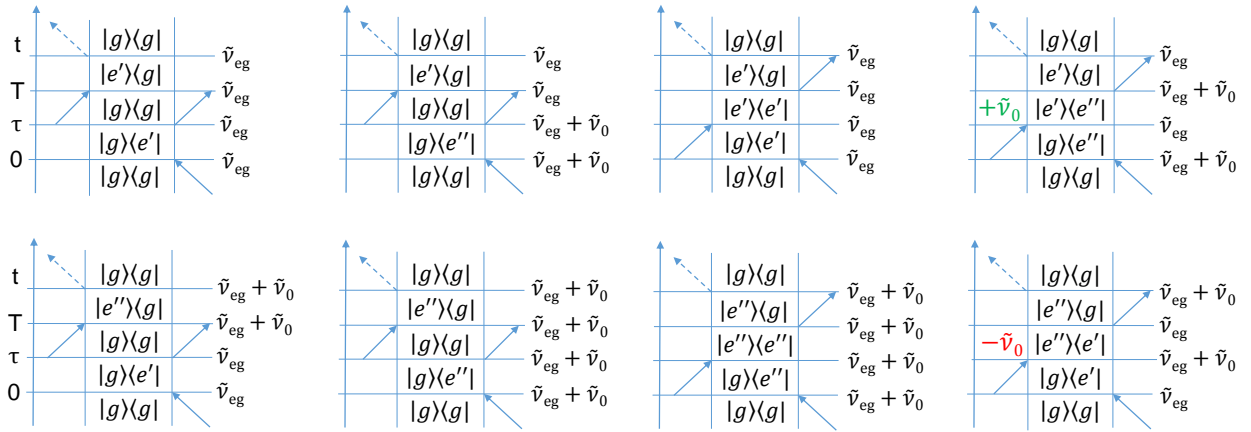


Figure S10. Rephasing Liouville-space pathways for the energy level scheme in Figure 2b.

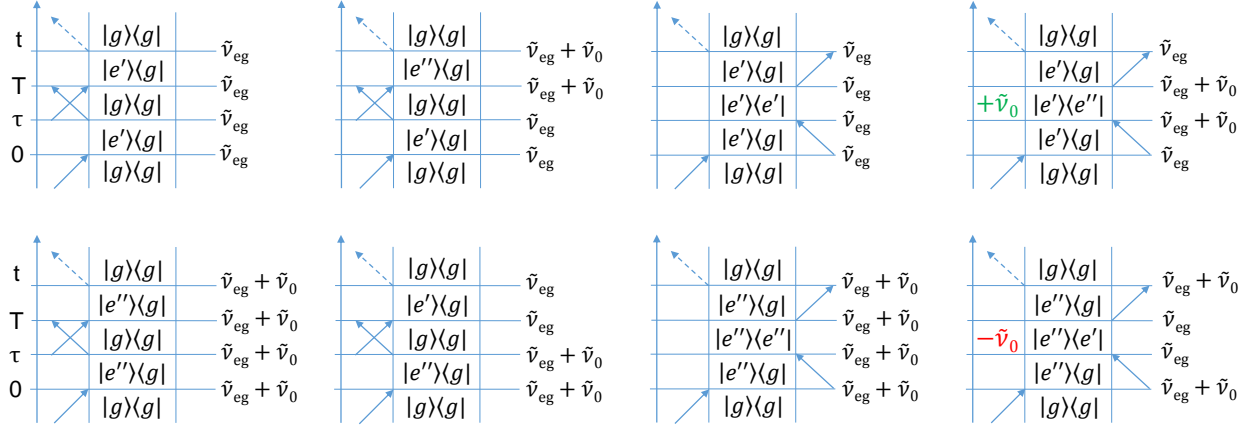


Figure S11. Non-rephasing Liouville-space pathways for the energy level scheme in Figure 2b.

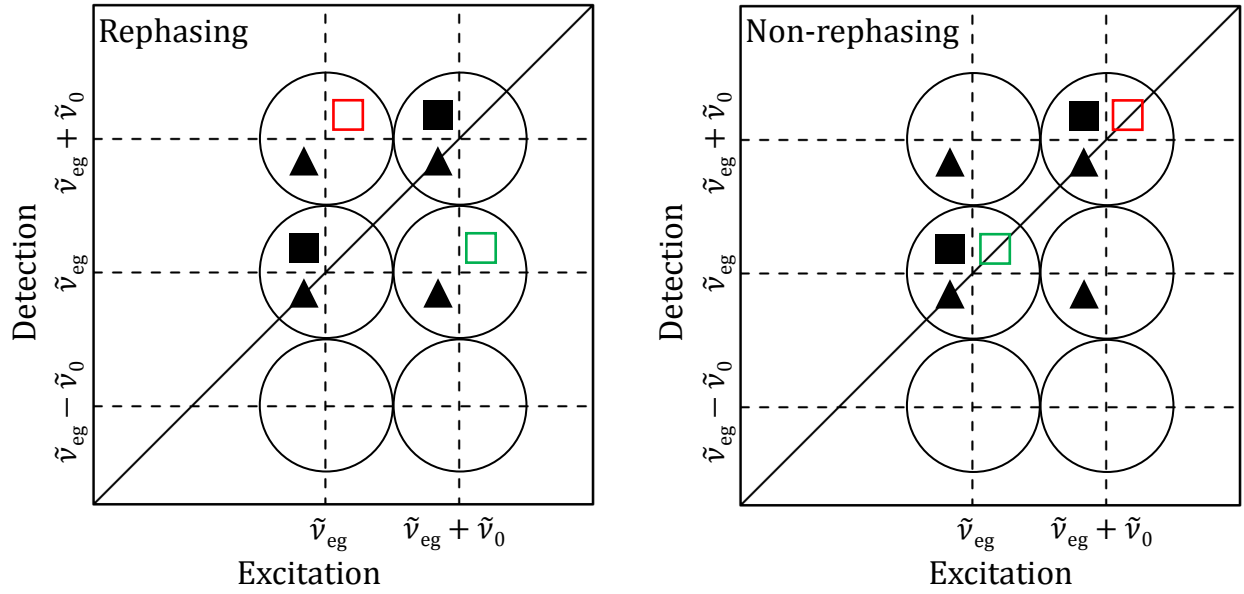


Figure S12. Scheme of Liouville-space pathways in a rephasing (left) and non-rephasing (right) 2D maps for the energy level structure shown in Figure 2b. See caption of Figure S7 for details.

EXPERIMENT 1

In this section we show supplemental material for the 2D-ES experiment 1 from the main text. In Figure S13 the real and imaginary parts of the rephasing spectrum at $T = 70$ fs are shown, and in Figure S14 the real and imaginary parts of the non-rephasing spectrum at the same population time are shown. The color scale is symmetric and has the maximum value corresponding to the darkest tone of red in each map. In experiment 1 the laser spectrum covers mostly the absorption of the sample below 16400 cm^{-1} , where it is dominated by the main electronic transition at 15650 cm^{-1} , along with the vibronic shoulder associated with the 375 cm^{-1} vibrational mode. We highlight that the measured data for this relatively simple case compares well to calculated real and imaginary rephasing and non-rephasing spectra for a single electronic transition found in the literature, reinforcing our ability to reliably recover real and imaginary parts with our 2D-ES setup [9].

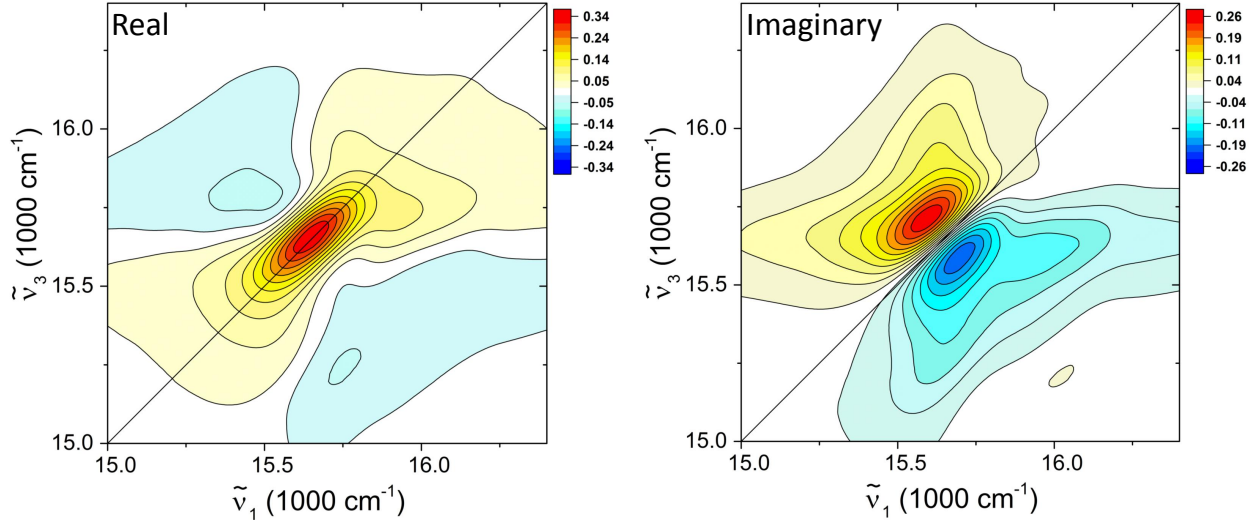


Figure S13. Real and imaginary rephasing maps for experiment 1 at $T = 70$ fs.

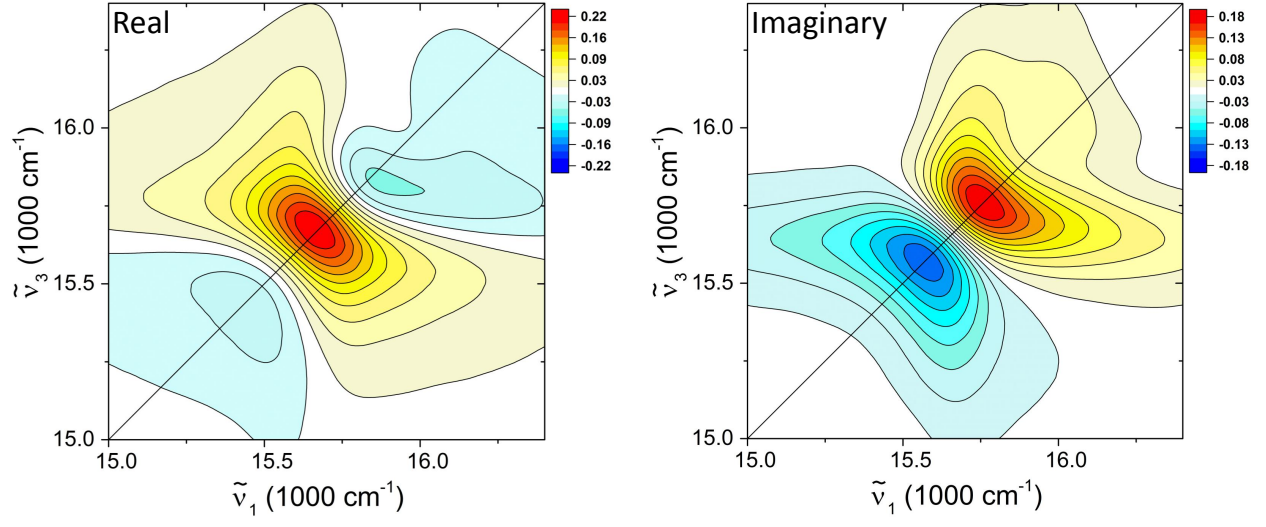


Figure S14. Real and imaginary non-rephasing maps for experiment 1 at $T = 70$ fs.

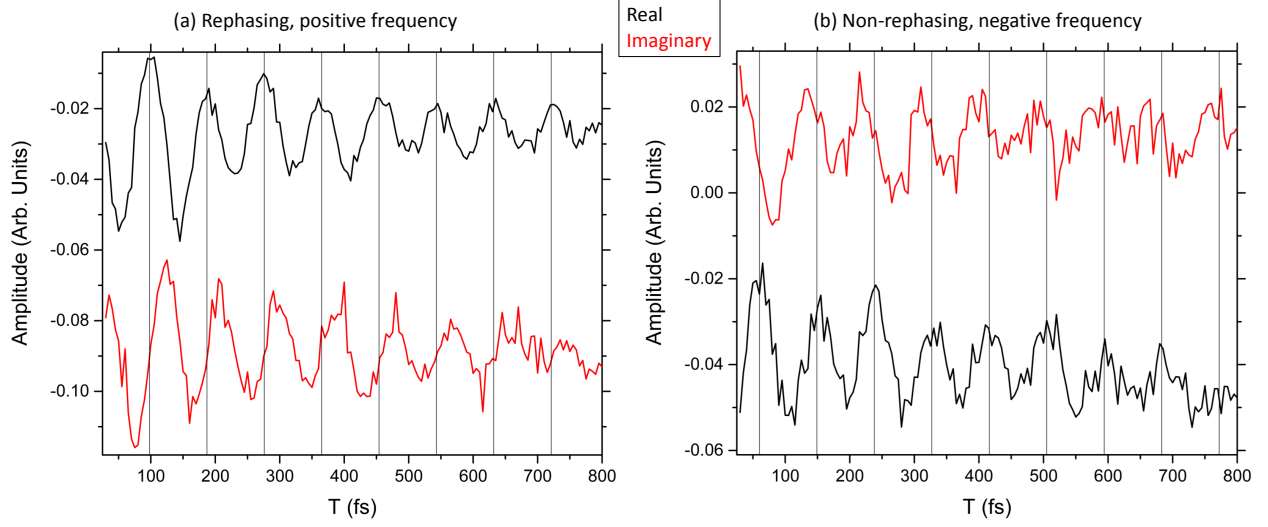


Figure S15. **(a)** Real (black) and imaginary (red) rephasing traces as a function of T for $\tilde{\nu}_1 = 15725 \text{ cm}^{-1}$ and $\tilde{\nu}_3 = 15295 \text{ cm}^{-1}$ in experiment 1. At this point the only coherences expected and detected at 375 cm^{-1} have positive frequency, which corresponds to an oscillation like $\cos(\tilde{\nu}_0 T) + i \sin(\tilde{\nu}_0 T)$ in the time domain – that is, the maxima of the imaginary part will be delayed by $\frac{\pi}{2}$ compared to the real part, in agreement with the observations. A factor of 0.05 was subtracted from the imaginary part to avoid overlap between the graphs. **(b)** Real (black) and imaginary (red) non-rephasing traces as a function of T for $\tilde{\nu}_1 = 15955 \text{ cm}^{-1}$ and $\tilde{\nu}_3 = 15918 \text{ cm}^{-1}$ in experiment 1, where only coherences of negative frequencies at 375 cm^{-1} are forecast and detected, corresponding to an oscillation like $\cos(\tilde{\nu}_0 T) - i \sin(\tilde{\nu}_0 T)$ in the time domain – a $\frac{\pi}{2}$ shift in the opposite direction to that observed in (a). A factor of 0.035 was subtracted from the imaginary part to bring the traces closer together.

EXPERIMENT 2

In this section we present supplemental material for the 2D-ES experiment 2 from the main text. Experiment 2 is intrinsically more complex than experiment 1, because the laser now partially covers the second absorption peak in the Q band. We have reported in a previous 2D-ES study of this molecule that significant excited state absorption (ESA) occurs from the Q band to the N band, as the energy gaps between the ground state and Q and between Q and the N band are similar [10]. The spectrum used in experiment 2 favours the ESA pathways more than that of experiment 1, and the broad character of the N band implies that ESA contributions will be spread throughout the $(\tilde{\nu}_1, \tilde{\nu}_3)$ plane. As a result of these overlapping positive and negative features, the 2D-ES lineshapes are no longer readily comparable to usual models. For completeness, we show in Figures S16 and S17 the rephasing and non-rephasing maps at $T = 70$ fs. Nonetheless, the presence of the extra ESA pathways to the broad N band should not substantially affect the analysis of the oscillations in the region we are interested in.

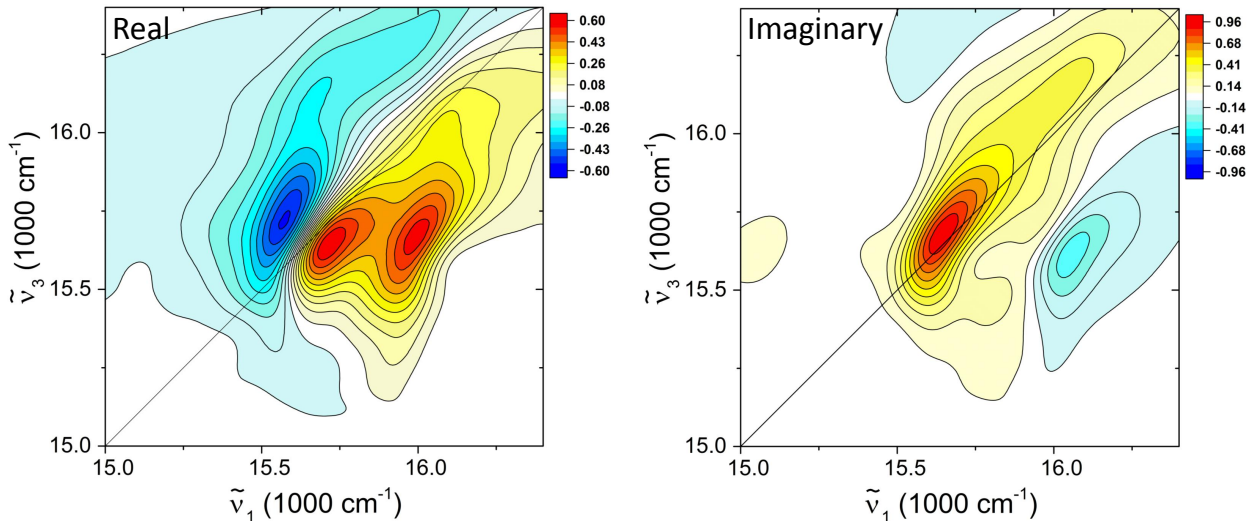


Figure S16. Real and imaginary rephasing maps for experiment 2 at $T = 70$ fs.

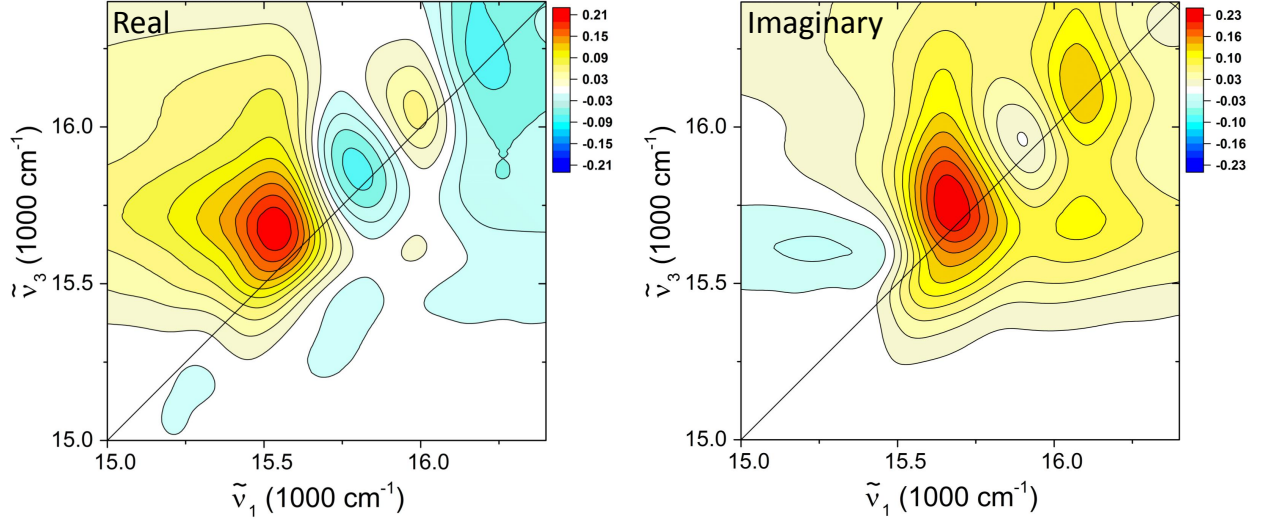


Figure S17. Real and imaginary non-rephasing maps for experiment 2 at $T = 70$ fs.

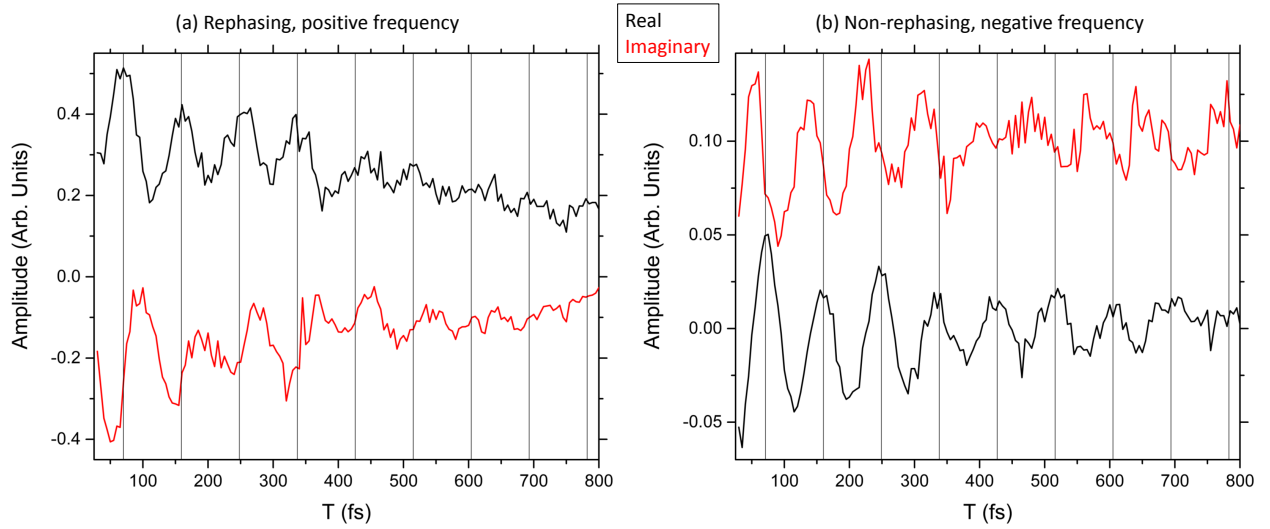


Figure S18. **(a)** Real (black) and imaginary (red) rephasing traces from experiment 2 as a function of T for $\tilde{\nu}_1 = 16025 \text{ cm}^{-1}$ and $\tilde{\nu}_3 = 15650 \text{ cm}^{-1}$, corresponding to the expected central position of the Liouville-space pathways with $\tilde{\nu}_2 = +375 \text{ cm}^{-1}$ – the phase shift expected for positive frequencies is observed. **(b)** Real (black) and imaginary (red) non-rephasing traces from experiment 2 as a function of T for $\tilde{\nu}_1 = \tilde{\nu}_3 = 16025 \text{ cm}^{-1}$, corresponding to the expected central position of the Liouville-space pathways with $\tilde{\nu}_2 = -375 \text{ cm}^{-1}$ – the phase shift expected for negative frequencies is observed.

-
- [1] D. Koszelewski, A. Nowak-Krol, M. Drobizhev, C. J. Wilson, J. E. Haley, T. M. Cooper, J. Romiszewski, E. Gorecka, H. L. Anderson, A. Rebane, and D. T. Gryko, *Journal of Materials Chemistry C* **1**, 2044 (2013).
- [2] M. Drobizhev, Y. Stepanenko, Y. Dzenis, A. Karotki, A. Rebane, P. N. Taylor, and H. L. Anderson, *The Journal of Physical Chemistry B* **109**, 7223 (2005).
- [3] I. A. Heisler, R. Moca, F. V. A. Camargo, and S. R. Meech, *Review of Scientific Instruments* **85**, 063103 (2014).
- [4] F. D. Fuller and J. P. Ogilvie, *Annual Review of Physical Chemistry*, **66**, 667 (2015).
- [5] U. Selig, F. Langhojer, F. Dimler, T. Loehrig, C. Schwarz, B. Giesekeing, and T. Brixner, *Optics Letters* **33**, 2851 (2008).
- [6] M. L. Cowan, J. P. Ogilvie, and R. J. D. Miller, *Chemical Physics Letters* **386**, 184 (2004).
- [7] P. Hamm and M. Zanni, *Concepts and methods of 2D infrared spectroscopy* (Cambridge University Press, 2011).
- [8] V. Butkus, D. Zigmantas, L. Valkunas, and D. Abramavicius, *Chemical Physics Letters* **545**, 40 (2012).
- [9] V. Butkus, D. Abramavicius, A. Gelzinis, and L. Valkunas, *Lithuanian Journal of Physics* **50**, 267 (2010).
- [10] F. V. A. Camargo, H. L. Anderson, S. R. Meech, and I. A. Heisler, *The Journal of Physical Chemistry A* **119**, 95 (2015).